2011

A Physical Model for Non-ohmic Shunt Conduction and Metastability in Amorphous Silicon p-i-n Solar Cells

Sourabh Dongaonkar
Purdue University - Main Campus, sourabh@purdue.edu

Karthik Y
Indian Institute of Technology - Bombay

Souvik Mahapatra
Indian Institute of Technology - Bombay

Muhammad A. Alam
Network for Computational Nanotechnoloy, Birck Nanotechnology Center, School of Electrical and Computer Engineering, Purdue University

A PHYSICAL MODEL FOR NON-OHMIC SHUNT CONDUCTION AND METASTABILITY IN AMORPHOUS SILICON P-I-N SOLAR CELLS

Sourabh Dongaonkar[1], Karthik Y[2], Souvik Mahapatra[2], and Muhammad A Alam[1]
[1]Departmet of Electrical and Computer Engineering, Purdue University, W Lafayette, IN, USA
[2]Department of Electrical Engineering, IIT Bombay, Mumbai, MH, India

ABSTRACT

We present a physical model of non-ohmic shunt current (I_{SH}) in a-Si:H p-i-n solar cells, and validate it with detailed measurements. This model is based on space-charge-limited (SCL) transport through localized parasitic p-i-p shunt paths. Such paths can arise from n-contact metal incorporation in a-Si:H layer, causing the (n)a-Si:H to be counter doped to p-type. This model explains all the electrical characteristics of I_{SH} and provides insight into the metastable switching behavior of the shunts under an integrated framework. We first verify the SCL model using simulations and statistically robust measurements, and then use this picture to analyze our systematic observations of nonvolatile switching of shunt current caused by reverse bias sweeps. This work not only resolves broad experimental observations on shunt behavior, but also suggests possible techniques for alleviating shunt induced performance and reliability issues.

INTRODUCTION & BACKGROUND

Parasitic shunt leakage is responsible for significant loss in efficiency going from cell to panel level [1]; and loss of parametric yield for all PV technologies. Consequently, the issue of shunt leakage has been studied actively. Many shunts observed at the panel level have been correlated to localized, macroscopic (up to ~mm) non-uniformities (e.g., pinholes) on the solar cell surface. These pinhole defects have been identified with particulate debris on the panel surface during deposition, and can be minimized by better control of deposition conditions [2, 3]. However, even the cells that are fabricated with excellent process control and therefore generally free from such "extrinsic shunts", might still show substantial shunt currents [4]. Although these "intrinsic shunts" may not be visible to naked eye, they are visible distinctively as numerous bright spots in thermography maps [5].

Like the "extrinsic" shunts, the intrinsic shunts also introduce considerable performance variation among nominally identical cells. However, unlike the extrinsic shunts which are ohmic, the intrinsic shunts are typically characterized by symmetrical *non-ohmic* conduction. Moreover, these shunts also show a threshold switching behavior, which manifests as abrupt switching of shunt current at certain reverse voltage biases [6]. This threshold switching is well known in the PV industry, and is used for electrical shunt removal/reduction (shunt busting) [7]. However, the metastability of these shunts means that I_{SH} can also increase on application of reverse voltages. Under normal operation, such reverse bias can arise from partial shadowing of the panel, and can have significant impact on the long term panel output [8]. While the empirical features of intrinsic shunts have been known, a consistent physical model of shunt conduction is lacking. A complete understanding of shunt formation is therefore is important for preventing the variability and reliability issues caused by shunt leakage. Development of such a model, which can help in identifying shunt formation processes, is the goal of this contribution.

SPACE-CHARGE-LIMITED SHUNT CURRENT

Phenomenological Model

The identification of the physical mechanism of shunt conduction in an as-fabricated a-Si:H solar cells is the critical first step in addressing the problem. The three key phenomenological features of shunt current (I_{SH}) in a-Si:H cells reported in the literature are as follows: (i) large fluctuation in current magnitude from one cell to the next (Fig. 1a); (ii) symmetry of shunt current about V = 0, and (iii) non-ohmic, power-law, voltage dependence $I \sim V^{\beta}$ (Fig. 1b) [4].

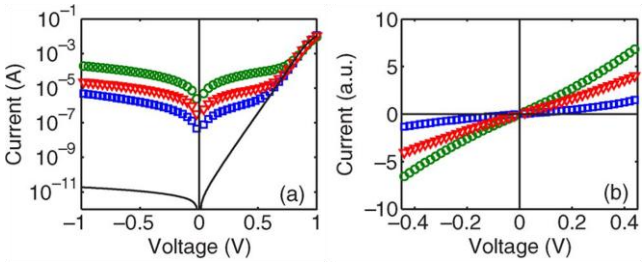

Fig. 1: (a) Variation in I_{SH} magnitude in 3 nominally identical devices (symbols); compared to identical diode current (solid line). (b) Symmetric non-ohmic behavior about V = 0 for the same 3 devices (scaled for clarity).

A phenomenological SCL current model was proposed to accounts for these features within a common framework [4]. SCL transport occurs in a symmetric (e.g., Metal/Semiconductor/Metal type) structure where only single carrier injection is possible (Fig. 2a). For materials with shallow traps, which are exponentially distributed in energy SCL current is given as:

$$I_{SCL} = A\varepsilon\mu_c(\gamma)\frac{V^{\gamma+1}}{L^{2\gamma+1}}. \quad (1)$$

Here, A is area, L is thickness, ε is the dielectric constant, and $\mu_c(\gamma)$ is the effective carrier mobility, and parameter γ

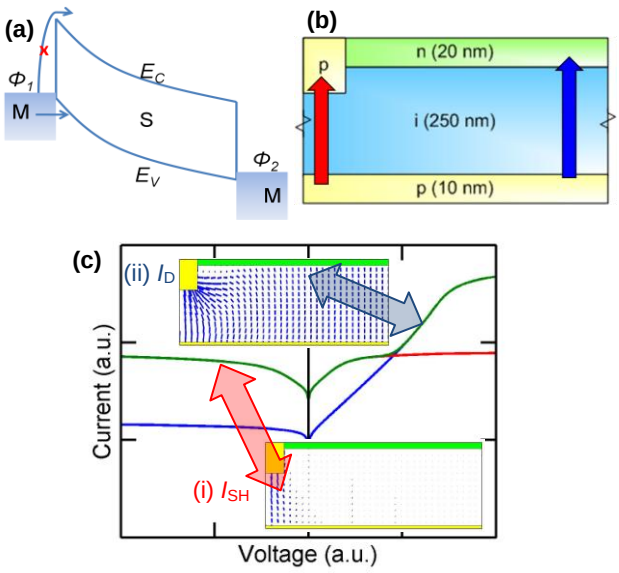

Fig.2: (a) Symmetric MSM type structure for SCL conduction showing single carrier injection. (b) Proposed local parasitic p-i-p structure in otherwise ideal p-i-n structure. (c) Dark IV from the 2D simulation showing that the shunt (red), and diode (blue) dominate in different voltage regimes to give the total dark current (green). Quiver plots in inset contrast localized current distribution in shunt dominated regime (i) with the uniform diode current conduction (ii).

is a function of trap distribution inside the bandgap [9]. It is apparent from (1) that symmetry and non-ohmic nature of I_{SH} can be explained readily by SCL conduction. However, the physical nature of shunt path responsible for SCL shunt is not apparent from this picture.

Localized p-i-p shunt

We now investigate a likely physical origin of the symmetric parasitic path responsible for an SCL shunt. A likely candidate for SCL shunt, in parallel to the bulk exponential diode current, is a localized p-i-p structure (Fig. 2b) anywhere in the cell. Such structure may form during the cell fabrication if Al from the top AZO layer diffuses into the a-Si:H layer to sufficient depth and counter-dopes it to p-type. Evidence of such possibility can be found in [10]. Strain induced cracks or voids in the a-Si:H layer, due to patterning of the substrate, may also facilitate Al diffusion at certain locations [11]. Since, the n-layer is just ~20nm, even a small Al incursion can result in a local p-i-p shunt path. Therefore, these shunt paths are not visible to naked eye, but will show up in thermography maps as light spots.

This localized p-i-p shunt hypothesis can be explored by numerical simulation. A self consistent simulation of this 2D structure, using commercial Medici™ software, readily reproduces the essential features of SCL shunt (Fig 2c). The SCL current through p-i-p shunt regions dominates in the lower bias regimes, while the exponential diode current through the p-i-n region takes over at higher forward biases. This transition can be visualized using the quiver plots of the current in Fig. 2c insets; in inset (i) the current is localized to p-i-p shunt region and is symmetric with voltage. At higher forward biases the p-i-n diode current becomes large enough, and the current distribution is more uniform across the device, as seen in inset (ii).

Another interesting insight from the quiver plots is that the shunt and diode currents are physically separated and dominate the conduction in different regimes. Therefore, we can avoid the computationally intensive 2D simulations by using separate 1D p-i-p shunt and p-i-n diode (Fig. 3a). The relative area of shunt region (sum over all the localized paths) with respect to total diode (cell) area will determine the shunt current magnitude. Fig. 3b shows that the separate 1D simulations of shunt and diode structures match the measured voltage and temperature dependencies of the dark IV cell very well.

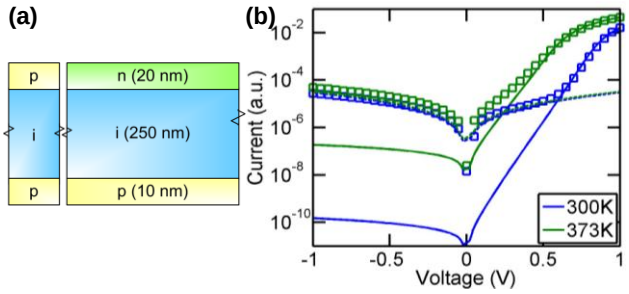

Fig. 3: (a) Separation of diode and shunt structures allows a 1D simplification, (b) the 1D simulations of shunt (dashed line) and diode (solid line), showing excellent match with dark IV-T data (symbols).

VALIDATION OF P-I-P SHUNT MODEL

While electrical features are satisfactorily reproduced by the p-i-p shunt model, a conclusive confirmation requires that the predictions of this model be independently verified. We investigate two such predictions next. First is that the p-i-p shunts must be dominated by hole conduction. And second is that SCL conduction must scale as L^{-n} where L is the thickness of the intrinsic layer. We will consider these two features in the following discussion.

Confirmation of hole transport

SCL conduction requires single carrier injection, and in the case of p-i-p shunt this implies hole injection in the i layer. While it is difficult to isolate hole current in 2-terminal measurements, we can indirectly establish the hole transport of I_{SH} by examining the power exponent ($\beta = \gamma+1$) in eq. (1). It has been shown that for materials with exponentially distributed shallow traps, the parameter γ is E_0/k_BT, where E_0 is the characteristic energy of the trap

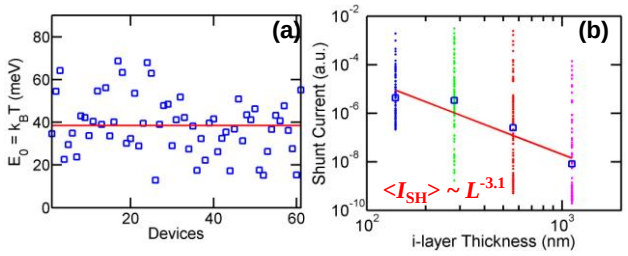

Fig 4: (a) Extracted characteristic slope of band tails using ($E_0 = \gamma kT = (\beta-1)kT$) is ~40 meV for 61 devices, which is close to the valence band tail slope in a-Si:H. (b) Length dependence of I_{SH} (at -1V) of devices with 4 different i-layer thicknesses. Colored dots represent individual devices (89 devices for each i-layer thickness), and show the statistical spread of shunt area. The geometric mean (squares) shows distinctly power law (~ $L^{-3.1}$) dependence, as expected from the SCL shunt model.

distribution [9]. This can be used to estimate the E_0 for a-Si:H in the p-i-p shunt as, $E_0 = \gamma k_B T = (\beta - 1)k_B T$. Fig. 4a shows that the calculated E_0 for 61 cells is ~40 meV. It is well known that the characteristic slope of valence band tail in a-Si:H is ~40-50 meV, as opposed to conduction band tail slope of ~20 meV [12]. This shows that the SCL shunt current is indeed due to injection of holes in i layer. This observation is consistent with the first prediction of the p-i-p shunt model.

Thickness dependence

Another feature of the non-ohmic SCL conduction from eq. (1) is that the SCL current scales inversely with thickness as a power law ($I \sim 1/L^{2\gamma+1}$). In case of shunt currents, the voltage power exponent β (= γ+1) is ~1.5-2.5, which means that the power exponent of thickness dependence must be between -3 and -4. To check this prediction, we measured 356 nominally identical devices, with i-layer thickness 140nm, 280nm, 560nm and 1120nm (89 devices of each thickness). In Fig. 3b the current at -1V vs. i-layer thickness is plotted for all measured devices, where each dot represents a separate device. We find that the geometric mean of the data $\langle I_{SH}(L) \rangle$ indeed shows a power law behavior, with power exponent ~-3.1, generally consistent with the SCL model.

The spread in shunt current values is over several orders of magnitude, which is consistent with the broad distribution of the number of shunt paths and/or shunt strength from device to device. It is important to note that this spread remains statistically similar for different i-layer thicknesses. This implies that while the magnitude of I_{SH} depends on i-layer thickness L, the probability of shunt formation does not. This observation also supports the p-i-p shunt model which is based on metal incorporation through the top n-layer. Since the n-layer thickness is same for all devices, the model anticipates the shunt formation probability (analogously the number/area of shunt paths per cell) should be independent of i-layer thickness, as apparent from the identical spread of the I_{SH} data for different i-layer thicknesses.

NON-VOLATILE SWITCHING

So far we have seen that the proposed p-i-p shunt model, with SCL current behavior, can explain the electrical features of shunt conduction in a coherent manner. We now show that this picture can also help us in understanding the nonvolatile switching in shunt current values caused by reverse voltage pulses or sweeps (Fig. 5a).

Threshold switching of shunts has been observed in literature for shunts in a-Si:H solar cells [6], and is also used in industry for “shunt busting” [7]. However, our measurements show that this switching is not just one way (from low to high resistance following shunt busting) but is actually *metastable*. We observe that during reverse voltage sweep, I_{SH} decreases abruptly by about 1-2 orders of magnitude (OFF transition), analogous to the shunt busting (Fig. 5a). This change in shunt current is nonvolatile during subsequent IV measurements. However, I_{SH} increases again (ON transition), after a subsequent reverse current sweep, and stays at the higher value thereafter. The abrupt transitions of I_{SH} during the two sweeps are shown Fig. 5b. Note that both these metastable states of shunt current are nonvolatile and remains stable for many days under room temperature storage.

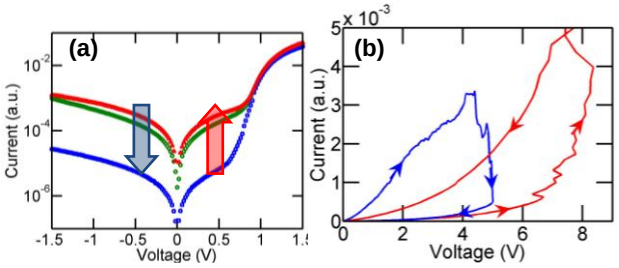

Fig. 5: (a) The initial dark IV (green), switches to low I_{SH} state after voltage sweep (blue), increases again after subsequent current sweep (red); and (b) the abrupt switching transitions during voltage sweep showing the OFF transition (blue), and current sweep showing ON transition (red).

Switching Thresholds for Transition

In order to investigate the statistical features of this switching behavior, we measured 16 nominally identical devices, applying reverse voltage and current sweeps. Consecutive voltage sweeps of -5V,-6V and -7V, and reverse current sweeps of 0.5mA, 5mA, and 50mA were applied to all devices. 8 devices were subjected first to voltage sweep followed by current sweeps, and the other 8 were stressed in opposite order. The sweep rate was kept at the fastest possible, with typical sweep time below 1s.

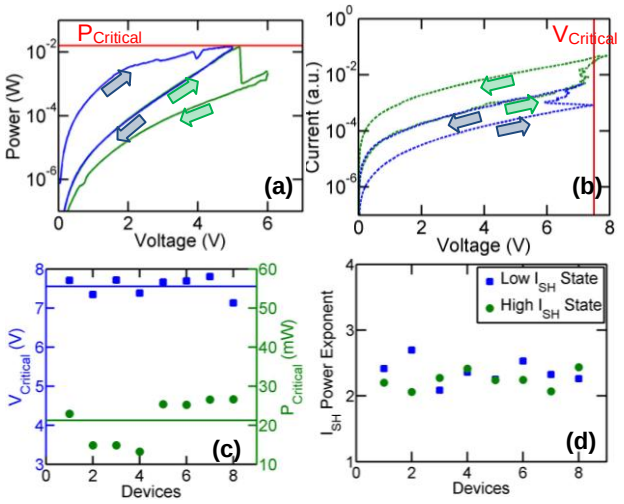

Fig. 6: Sweep data for an individual device showing that (a) the OFF transition is triggered at power threshold $P_{Critical}$, for 2 subsequent voltage sweeps, while (b) the ON transition is triggered at threshold voltage $V_{Critical}$ for 2 subsequent current sweeps. (c) Scatter plot showing that the values of $P_{Critical}$ and $V_{Critical}$ are similar for 8 devices. (d) Power exponent of SCL shunt current in the metastable devices, in the high (after ON) and low (after OFF) shunt current states shows no appreciable difference.

Of the 16 devices measured, 8 did not exhibit any change in shunt current. For the 8 devices, which show metastability, the switching showed distinct features for ON and OFF transitions. We found that the decrease in I_{SH} (OFF transition) was determined by a *power* threshold $P_{Critical}$ (Fig. 6a); on the other hand, the increase in I_{SH} (ON transition) was triggered at a threshold *voltage* $V_{Critical}$ (Fig. 6b). These thresholds were independent of the order in which the devices were stressed (voltage first then current or vice-versa). Fig. 6c shows the threshold voltage and power values for all the 8 metastable shunts are ~7.5V and ~20mW, respectively. And, Fig. 6d compares the SCL power exponent (β) of shunt under high current and low current states, showing them to be roughly identical. This shows that the nature of shunts does not change before and after switching.

Mechanism of ON transition

In order to analyze the metastable switching behavior, we can use the p-i-p shunt picture and explore the possible mechanisms. Note that only a small Al filament is sufficient to cause the SCL shunt and that I_{SH} increase is a voltage (or possibly electric field) triggered process, as seen in Fig. 6b. These observations suggest that the positively charged Al ions, from top AZO contact, might be hopping through the a-Si:H matrix under the influence of the electric field and migrating into a-Si:H layer. And, as Al gets past the thin n-layer, it will destroy the n-i junction locally and form a p-i-p shunt in its place. Since, Al needs to migrate only about 10-20 nm in order to form a p-i-p region (Fig. 7a), the ON transition (driven by large voltage) would be very rapid, as observed. Contact metal incorporation in a-Si:H matrix has been studied extensively in nonvolatile resistive switching memories made from amorphous silicon [13]. This behavior of Al (and other metals) migrating into a-Si:H under applied bias, in fact forms the basis of operation of these memories. Direct evidence for Al migration in a-Si:H matrix under bias is also available in memory literature [14]. Owing the similarities in materials (Al/a-Si:H) and the structures involved, it seems very likely that the similar physical processes are driving the ON transitions in metastable shunts also.

There are however certain distinctions; in case of a-Si:H based memories, the program/WRITE biases applied are substantially higher and the conduction is *ohmic* in ON state. This is because in memories the metal filament goes all the way through the bulk to form a short to the other contact. However, in case of shunt current switching, the power exponent of I_{SH} does not change significantly before and after the switching event (remaining close to 2). This suggests that the essential nature of shunt paths remains the same before and after ON/OFF transition. And, it appears only a small incursion of the metal ions inside the bulk takes place (enough to overcome the n-i junction), during the ON transition, as the conduction remains SCL afterwards. This means that the ohmic shunt path due to metal filament causing a short is not responsible for the ON transition. Moreover, the shunt current value after one ON and OFF transitions is not necessarily the same. Based on this we propose that the ON transition happens due to the formation of a new shunt path due to Al migration from the top contact AZO.

Mechanism of OFF transition

On the other hand, the OFF transition is a power driven process as seen in Fig. 6a. This is most probably caused by dissolution of the small Al filament due to local heating. Since, the sweep rates are high and shunt region is small, the local heating could be sufficient to dissolve/disperse the small filament responsible for shunt conduction. Another important factor is that the largest shunt path is carrying most of the current (Fig. 7b), so the local heating effect will affect the largest shunt. In a typical solar cell there are many localized shunt with different magnitudes, distributed randomly across cell surface. This has been established through thermography and luminescence imaging techniques [15]. From Fig. 4b we note that the magnitude of these shunts can vary by orders of magnitude from one cell to other. This distribution implies that even on a single cell there are many shunts with very different magnitudes. Typically only the largest shunt path (with lowest resistance) will dominate the total shunt current in a particular cell. Therefore, it is likely that the OFF transition is a result of the largest shunt path getting extinguished due to local heating, so that the total current is now due to the next largest shunt.

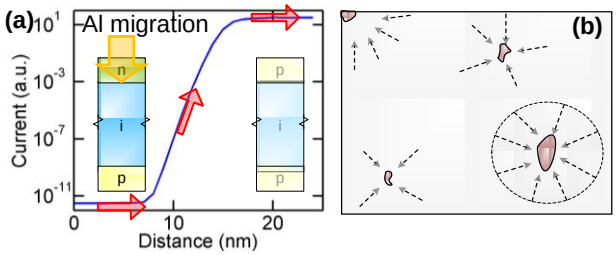

Fig. 7: (a) Simulations show sharp increase in reverse current vs. distance of Al incursion in n-layer, explains how I_{SH} might jump due to field driven Al migration; insets showing the initial p-i-n diode structure and final p-i-p shunt after Al incursion and counter-doping. (b) Schematic showing top view of a solar cell with different shunts, the largest one carries most of the current and hence, is subject to local heating.

While the physical nature of shunt metastability has its similarities to a-Si:H based nonvolatile memories; there is an important distinction due to the statistical distribution of preexisting shunts in solar cells. Nevertheless, we believe that the understanding of the physical processes of metal incorporation in a-Si:H matrix, obtained through the study of resistive memories, will definitely prove to be useful for the study of shunt behavior in thin-film solar cells. Further investigations on the nature of shunt formation in thin film solar cells should benefit from this picture of metal incorporation in semiconductor layers. We would also like to note that metastable behavior of shunt currents has also been observed in CdTe cells [16]. Since the SCL shunt model has been shown to be applicable to CIGS cells [17], and given the similar structures of CIGS and CdTe cells, the model developed here could also possible explain the metastable shunts in CdTe as well.

CONCLUSION

We have provided and validated a physics based model which can explain the electrical and metastable features of shunts in a-Si:H p-i-n solar cells. A physical understanding of shunt behavior enables one to explore possible solutions for shunting problems. For example, since Al migration appears to cause shunt formation, it might be useful to put a barrier layer between AZO and a-Si:H to block this migration. Moreover, the understanding of the metastable shunt behavior will enable a better understanding of the degradation of panel performance over time, caused by the increase of the shunt current. For example, the voltage triggered I_{SH} increase suggests that techniques for avoiding large reverse voltages caused by partial panel shading would be very important to avoid shunt degradation during panel operation. While further experiments are needed for constructing a complete picture of shunt physics, the model presented here should provide useful guidance for any such investigations in future.

ACKNOWLEGMENT

This work was funded by SRC-ERI Network for Photovoltaic technology. M. A. A. was supported as a part of EFRC, funded by the US Department of Energy, Award Number DE-SC0001085. We would also like to thank Dr. M Frei & Dr. D Wang from Applied Materials discussions and support.

REFERENCES

[1] G. T. Koishiyev and J. R. Sites, "Effect of shunts on thin-film CdTe module performance," in *Materials Research Society Symposium*, 2009, pp. 203-208.

[2] B. G. Yacobi, T. J. McMahon, and A. Madan, "Electron-beam-induced current microcharacterization of fabrication defects in hydrogenated amorphous silicon solar cells," *Solar Cells,* vol. 12, pp. 329-335, 1984.

[3] O. Kunz, J. Wong, J. Janssens, J. Bauer, O. Breitenstein, and A. G. Aberle, "Shunting problems due to sub-micron pinholes in evaporated solid-phase crystallised poly-Si thin-film solar cells on glass," *Progress in Photovoltaics: Research and Applications,* vol. 17, pp. 35-46, 2009.

[4] S. Dongaonkar, K. Y, D. Wang, M. Frei, S. Mahapatra, and M. A. Alam, "On the Nature of Shunt Leakage in Amorphous Silicon p-i-n Solar Cells," *Electron Device Letters, IEEE,* vol. 31, pp. 1266-1268, 2010.

[5] K. Bothe, K. Ramspeck, D. Hinken, C. Schinke, J. Schmidt, S. Herlufsen, R. Brendel, J. Bauer, J. M. Wagner, N. Zakharov, and O. Breitenstein, "Luminescence emission from forward- and reverse-biased multicrystalline silicon solar cells," *Journal of Applied Physics,* vol. 106, pp. 104510-8, 2009.

[6] K. R. Lord, M. R. Walters, and J. R. Woodyard, "Investigation Of Shunt Resistances In Single-Junction A-Sih Alloy Solar Cells," in *Materials Research Society Symposium*, 1994, pp. 729-734.

[7] G. E. J. Nostrand, NJ), Hanak, Joseph J. (Lawrenceville, NJ), "Method of removing the effects of electrical shorts and shunts created during the fabrication process of a solar cell," United States: RCA Corporation (New York, NY), 1979.

[8] S. Dongaonkar, Y. Karthik, D. Wang, M. Frei, S. Mahapatra, and M. A. Alam, "Identification, Characterization and Implications of Shadow Degradation in Thin Film Solar Cells,", in *IEEE International Reliability Physics Symposium (IRPS) 2011*, pp. 557-561.

[9] A. Rose, "Space-charge-limited currents in solids," *Physical Review,* vol. 97, pp. 1538-1544, 1955.

[10] M. S. Haque, H. A. Naseem, and W. D. Brown, "Aluminum-induced degradation and failure mechanisms of a-Si:H solar cells," *Solar Energy Materials and Solar Cells,* vol. 41-42, pp. 543-555, 1996.

[11] T. N. Ng, W. S. Wong, R. A. Lujan, and R. A. Street, "Characterization of charge collection in photodiodes under mechanical strain: Comparison between organic

bulk heterojunction and amorphous silicon," *Advanced Materials,* vol. 21, pp. 1855-1859, 2009.
[12]R. A. Street, *Hydrogenated amorphous silicon*. Cambridge; New York: Cambridge University Press, 1991.
[13]A. E. Owen, P. G. L. Comber, J. Hajto, M. J. Rose, and A. J. Snell, "Switching in amorphous devices," *International Journal of Electronics,* vol. 73, pp. 897 - 906, 1992.
[14]J. W. Seo, S. J. Baik, S. J. Kang, Y. H. Hong, J.-H. Yang, L. Fang, and K. S. Lim, "Evidence of Al induced conducting filament formation in Al/amorphous silicon/Al resistive switching memory device," *Applied Physics Letters,* vol. 96, pp. 053504-3, 2009.
[15]O. Breitenstein, J. P. Rakotoniaina, S. Neve, M. A. Green, Z. Jianhua, W. Aihua, and G. Hahn, "Lock-in thermography investigation of shunts in screen-printed and PERL solar cells," in *Twenty-Ninth IEEE PVSC*, 2002, pp. 430-3.
[16]A. Fahrenbruch, "Current transients in CdS/CdTe solar cells," in *Materials Research Society Symposium*, 2005, pp. 355-60.
[17]S. Dongaonkar, J. D. Servaites, G. M. Ford, S. Loser, J. E. Moore, R. M. Gelfand, H. Mohseni, H. W. Hillhouse, R. Agrawal, M. A. Ratner, T. J. Marks, M. S. Lundstrom, and M. A. Alam, "Universality of non-Ohmic shunt leakage in thin-film solar cells," *Journal of Applied Physics,* 2010.